Biophysical calculation of cell survival probabilities using amorphous track structure models for heavy-ion irradiation

2008 Phys. Med. Biol. 53 37

(http://iopscience.iop.org/0031-9155/53/1/003)

IOP Publishing Physics in Medicine and Biology

Phys. Med. Biol. **53** (2008) 37–59 doi:10.1088/0031-9155/53/1/003

Biophysical calculation of cell survival probabilities using amorphous track structure models for heavy-ion irradiation

Yuki Kase[1], Tatsuaki Kanai[1], Naruhiro Matsufuji[1], Yoshiya Furusawa[1], Thilo Elsässer[2] and Michael Scholz[2]

[1] Research Center for Charged Particle Therapy, National Institute of Radiological Sciences, Chiba 263-8555, Japan
[2] Biophysics, Gesellschaft für Schwerionenforschung, Planckstr. 1, 64291 Darmstadt, Germany

E-mail: y_kase@nirs.go.jp

Received 5 June 2007, in final form 30 October 2007
Published 12 December 2007
Online at stacks.iop.org/PMB/53/37

Abstract

Both the microdosimetric kinetic model (MKM) and the local effect model (LEM) can be used to calculate the surviving fraction of cells irradiated by high-energy ion beams. In this study, amorphous track structure models instead of the stochastic energy deposition are used for the MKM calculation, and it is found that the MKM calculation is useful for predicting the survival curves of the mammalian cells *in vitro* for ^{3}He-, ^{12}C- and ^{20}Ne-ion beams. The survival curves are also calculated by two different implementations of the LEM, which inherently used an amorphous track structure model. The results calculated in this manner show good agreement with the experimental results especially for the modified LEM. These results are compared to those calculated by the MKM. Comparison of the two models reveals that both models require three basic constituents: target geometry, photon survival curve and track structure, although the implementation of each model is significantly different. In the context of the amorphous track structure model, the difference between the MKM and LEM is primarily the result of different approaches calculating the biological effects of the extremely high local dose in the center of the ion track.

(Some figures in this article are in colour only in the electronic version)

1. Introduction

High-energetic heavy-ion beams offer excellent conditions for a highly conformal treatment of malignant tumors due to their favorable physical properties and their increase of the relative biological effectiveness (RBE) with penetration depth. During the years 1977 to 1993, helium-, carbon-, neon-, silicon- and argon-ion beams were clinically applied as cancer therapy at

the Lawrence Berkley National Laboratory (LBNL) in the United States (Tobias *et al* 1973, Pirruccello and Tobias 1980). In 1994, carbon-ion beams came into clinical use with the Heavy-ion Medical Accelerator in Chiba (HIMAC), located at the National Institute of Radiological Sciences (NIRS) in Japan (Hirao *et al* 1992). Carbon-ion radiotherapy has also been carried out since 1997 at the Gesellschaft fůr Schwerionenforschung mbH (GSI) in Germany (Kraft 2000) and since 2002 at the Hyogo Ion Beam Medical Center in Japan (Itano *et al* 1995, Kagawa *et al* 2005).

In the treatment planning of heavy-ion radiotherapy, it is necessary to calculate the biological dose, which is defined as the product of the absorbed physical dose and the RBE value at a certain position. However, the accurate calculation of the RBE value is difficult, because biological effects are related to extremely complex processes at various physical, chemical and biological stages. Presently, there are two different methods employed at the NIRS and the GSI that are used to predict the RBE value for applications in clinical carbon-ion radiotherapy.

At the GSI, Scholz and Kraft presented the local effect model (LEM) to predict the biological effect of heavy-ion beams (Scholz and Kraft 1996, Scholz *et al* 1997, Kraft *et al* 1999). In the case of the LEM, the biological effect is calculated by taking the x-ray survival curve as an input to determine the resulting damage from the local dose deposited by the charged particle tracks, which is derived from an amorphous track structure model. Krämer and Scholz (2000, 2006) incorporated the LEM into their treatment planning system for ion therapy (TRiP).

At the NIRS, different RBE values are used for clinical and radiobiological endpoints. The biological dose was defined as the product of the physical absorbed dose and the RBE at the 10% surviving fraction of *in vitro* human salivary gland (HSG) tumor cells (Kanai *et al* 1997). The clinical dose (GyE), which means a clinical RBE-weighted dose, has been used in the treatment planning of carbon-ion therapy in Japan (Kanai *et al* 2006). The NIRS-defined clinical dose distribution was calculated by normalizing the biological dose distribution to be adapted to the clinical RBE of neutron therapy (Kanai *et al* 1999).

Hawkins (1994, 2003) presented the microdosimetric kinetic model (MKM), which was developed out of the theory of dual radiation action (Kellerer and Rossi 1978, Zaider and Rossi 1980) in order to estimate cell survival after exposure to a heavy-ion beam. Kase *et al* (2006) revealed that the MKM can estimate the survival curves of human cells from the microdosimetric quantities measured with a spherical proportional counter, and these estimations can be carried out even for the complex radiation field of energetic heavy-ion beams from protons to silicon ions. Therefore, it might be a good candidate for RBE predictions in the framework of heavy ion treatment planning.

The MKM and LEM have conceptual similarities as follows:

(a) the principal target is the cell nucleus for any radiation quality,
(b) the nucleus is divided into small independent subvolumes,
(c) a cell survival curve for x-rays is adopted as the local dose-effect curve of each subvolume,
(d) the summation of the local effect in all subvolumes over the whole nucleus determines the cell survival probability.

The size of the subvolumes and the dose-effect curves are different between the MKM and LEM. In principle, the MKM focuses on the stochastic energy deposition in a micron-size domain while the LEM considers the local dose of infinitesimally small regions. Therefore, in MKM, the cell survival curve can be simulated from the experimentally obtained specific energy spectra obtained by a microdosimetric approach while the LEM uses a theoretical amorphous track structure model. In this study, we attempted to calculate the microdosimetric

specific energy from a track structure model in order to compare the MKM with the LEM calculation results using the same input data of amorphous track structure. We concentrated our comparison of models and experimental data on the original representation of the LEM, since this is the representation currently used in treatment planning for heavy-ion tumor therapy. However, in order to provide a thorough consideration of the model differences, we also present the results of a recently published modification of the LEM, which takes into account cluster effects at high local doses (Elsässer and Scholz 2007). For the MKM calculation, the microdosimetric specific energy of a cylindrical domain was derived from an amorphous track structure. It was found that the MKM can describe the published empirical data of *in vitro* HSG, V79 and T1 tumor cells irradiated by ^{3}He-, ^{12}C- and ^{20}Ne-ion beams (Furusawa *et al* 2000). The conceptual relation and differences between the MKM and the LEM are discussed below.

2. Materials and methods

2.1. Biophysical model of cell inactivation

In both the MKM and LEM, the cellular survival fraction is equal to the probability that the number of lethal lesions is zero in the cellular nucleus. When the distribution of lesion number in the nucleus is assumed to be the Poisson distribution, the survival fraction, S, is calculated as follows:

$$S = \exp(-\langle L_{\mathrm{nucl}}\rangle), \tag{1}$$

where $\langle L_{\mathrm{nucl}}\rangle$ is the cellular population averaged number of lesions in the nucleus.

2.1.1. Calculation of the lesion number in MKM. The cell nucleus is partitioned into microscopic-sized domains in the MKM. The specific energy of the domain, z, is the sum of the single-event specific energy, z_1, of this domain as follows:

$$z = \sum_{\mathrm{event}} z_1. \tag{2}$$

The value of z_1 can be obtained by either microdosimetry or by physical model calculations. The number of lesions in the nucleus is calculated as the sum of the number of lesions in all domains included in the nucleus. It is assumed that the number of lesions in the domain is given by the linear quadratic function of the specific energy, $Az + Bz^2$, for any radiation type. The linear-quadratic parameters, A and B, are dependent on cell type. The number of lesions in the nucleus, L_{nucl}, is given as follows:

$$\begin{aligned} L_{\mathrm{nucl}} &= \sum_{\mathrm{nucl}} (Az + Bz^2) \\ &= n\langle Az + Bz^2\rangle_{\mathrm{nucl}} \\ &= nA\langle z\rangle_{\mathrm{nucl}} + nB\langle z^2\rangle_{\mathrm{nucl}}. \end{aligned} \tag{3}$$

When the Poisson distribution is assumed for the event number of the domain, the cellular-population averaged number of lesions in the nucleus, $\langle L_{\mathrm{nucl}}\rangle$, is calculated as follows:

$$\begin{aligned} \langle L_{\mathrm{nucl}}\rangle &= \alpha_0\langle\langle z\rangle_{\mathrm{nucl}}\rangle + \beta\langle\langle z^2\rangle_{\mathrm{nucl}}\rangle \\ &= \alpha_0 D + \beta(z_{1D}D + D^2) \\ &= (\alpha_0 + \beta z_{1D})D + \beta D^2, \end{aligned} \tag{4}$$

where α_0 and β indicate nA and nB, D is the absorbed dose and z_{1D} is the single-event dose mean specific energy of the domain, as described below.

$$z_{1D} = \frac{\int_0^\infty z^2 f_1(z)\,\mathrm{d}z}{\int_0^\infty z f_1(z)\,\mathrm{d}z}, \tag{5}$$

where $f_1(z)$ is the probability density of z deposited by single energy deposition events of the domain.

2.1.2. Calculation of the lesion number in the LEM. In the LEM, the cell nucleus is partitioned into infinitesimally small volumes. The average number of lesions in the nucleus is assumed to be the integral of the number of lesions locally determined by referring to the empirical dose-lesion curve for x-rays, $L_{\mathrm{nucl},X}(d)$, for each infinitesimal volume. Here, it is assumed that the radiation effect of ion irradiation of a certain *local dose*, d, within this small volume corresponds to the effect of the same macroscopic dose, D, of photon irradiation. Then, the cellular-population averaged number of lesions in a nucleus, $\langle L_{\mathrm{nucl}}\rangle$, is obtained as follows:

$$\langle L_{\mathrm{nucl}}\rangle = \int_{\mathrm{nucl}} L_{\mathrm{nucl},X}(d)\,\mathrm{d}V \Big/ \int_{\mathrm{nucl}} \mathrm{d}V. \tag{6}$$

The dose-lesion curve for x-rays, $L_{\mathrm{nucl},X}(d)$, is divided into two different regions around the threshold dose, D_t, as follows:

$$L_{\mathrm{nucl},X}(d) = \alpha_X d + \beta_X d^2 \qquad (d \leqslant D_t), \tag{7}$$

$$L_{\mathrm{nucl},X}(d) = (\alpha_X + 2\beta_X D_t)d - \beta_X D_t^2 \qquad (d > D_t). \tag{8}$$

The modification of the linear-quadratic shape of the survival curve to a linear function of d at doses larger than D_t is based on the fact that experimental cellular survival curves on a logarithmic scale become linear in the high-dose region (Fertil *et al* 1994).

2.1.3. Correction due to non-Poisson distribution of lethal events. A correction of the non-Poisson lethal event distribution is necessary to predict the biological response in the case of a high LET ion track. In both models, the alpha value, which defines the initial slope of the survival curve, is the linear coefficient of the dose response curve for an infinitesimally small dose. In the case of high-LET radiation in the limit of low dose, nuclei with no hits or one hit must be considered in the equation of the survival fraction, while the percentage of nuclei hit by more than two particles is negligible. Thus, the survival fraction, $S(D)$, is given for monochromatic beams as follows:

$$S(D) = (1 - \phi \cdot D) + S_1 \phi \cdot D, \tag{9}$$

where ϕ is the hit probability per dose to a nucleus and S_1 indicates the survival fraction for a single hit to the nucleus. Thus, the corrected alpha value, α^*, is the linear coefficient of a dose, which gives the following equation:

$$\alpha^* = (1 - S_1)\phi. \tag{10}$$

In the case of the MKM (Hawkins 2003), the following equations are used in approximation:

$$\phi \cong (\alpha_0 + \beta \cdot z_{1D})/L(z_{1Dn}), \tag{11}$$

$$S_1 \cong \exp(-L(z_{1Dn})), \tag{12}$$

where z_{1Dn} is the single-event dose mean specific energy of the cell nucleus and $L(D)$ is the same function of $\langle L_{\text{nucl}} \rangle$ as that given in equation (4) for a given dose, D. Then, the α^* value is given as follows,

$$\alpha^* \cong (1 - \exp(-L(z_{1Dn}))) \left(\frac{\alpha_0 + \beta z_{1D}}{L(z_{1Dn})} \right). \tag{13}$$

According to Hawkins (2003), $L(z_{1Dn}) = (\alpha_0 + \beta z_{1D})\, z_{1Dn}$ and $z_{1Dn} = 0.16\text{LET}_\infty/A$, where LET_∞ is the unrestricted linear energy transfer in keV μm^{-1} for the incident particle and A is the area of the cell nucleus in μm^2, assuming $\rho = 1$ g cm^{-3} for the density of water. By assuming $A = \pi R_n^2$, equation (13) becomes the following equation:

$$\alpha^* \cong (1 - \exp L(z_{1Dn})) \frac{\rho \pi R_n^2}{LET_\infty}. \tag{14}$$

In the case of the LEM approximation (Elsässer and Scholz 2007, Scholz *et al* 1997), the following equations are used:

$$\phi \cong 0.16 \rho A / LET_\infty, \tag{15}$$

$$S_1 \cong \exp(-L_{\text{center}}), \tag{16}$$

where L_{center} describes the average number of lethal events generated by a particle traversing the center of the nucleus. Thus, α^* yields the same equation as expressed in equation (14), with the only difference being that the average number of lethal events for a single particle track is determined by a particle traversing along the center of the cell nucleus (Scholz *et al* 1997).

Therefore, the correction for the non-Poisson distribution of lethal events within the cell nucleus is determined by considering the Poisson distribution of the hit probability among cell nuclei yielding the same correction of α^* for both models. The difference between determinations of the averaged number of lethal events for a single particle track originates from the use of different concepts for the track structure and the dose. This difference is not a manifestation of the use of different methods of correction.

2.2. Track structure

Track structure represents the radial dose distribution around the trajectory of charged particles. To date, no comprehensive track structure model has been reported, because empirical examination is very difficult, particularly around a track core region on the order of a few nanometers. In this study, two amorphous track structure models were used for both the MKM and LEM calculations. Incorporating the track structure model into the MKM analysis is a new effort to calculate the ion dependence of LET-RBE curves by the MKM.

2.2.1. Track structure of the Kiefer–Chatterjee model. The first track-structure model is obtained by a combination of the Kiefer model for the penumbra region (Kiefer and Straaten 1986) and the Chatterjee model for the core radius (Chatterjee and Schaefer 1976). The core radius, R_c; the penumbra radius, R_p; the constant core dose, D_c; and the penumbra dose, D_p, as a function of track radius, r (μm), are calculated as follows:

$$R_c = 0.0116 \beta_{\text{ion}} \quad [\mu\text{m}], \tag{17}$$

$$R_p = 0.0616 \left(\frac{E}{A} \right)^{1.7} \quad [\mu\text{m}], \tag{18}$$

$$D_p(r) = 1.25 \times 10^{-4} \left(\frac{z^*}{b}\right)^2 r^{-2} \equiv K_p r^{-2} \quad \text{[Gy]}, \tag{19}$$

$$D_C = \frac{1}{\pi R_c^2}\left(\frac{LET_\infty}{r} - 2\pi K_p \ln\left(\frac{R_p}{R_c}\right)\right) \quad \text{[Gy]}. \tag{20}$$

where E is the energy, A is the mass, z^* is the effective charge given with the Barkas expression, β_{ion} is the velocity relative to the light velocity, LET_∞ is the unrestricted linear energy transfer for the incident ion and ρ is the mass density of water. This Kiefer–Chatterjee model is effective for explaining the responses of the diamond detector to heavy-ion beams (Sakama *et al* 2005). However, this model does not take into account the dispersion of the dose by the diffusion of radicals produced by radiolysis. Such indirect damage caused by radicals is relevant to generating DNA damage for low-LET as well as for high-LET radiation.

2.2.2. Track structure according to LEM. The second track structure model is the LEM-oriented track structure introduced by Scholz and Kraft (1996). This track structure model is used to calculate the local dose in the cell nucleus. Similar to the representation in the Chatterjee model, the dose in the track center is assumed to be constant, whereas in contrast to the Chatterjee model, there is no salient core region. In order to account for the radical diffusion, a center radius $R_c = 10$ nm is chosen below which the dose is constant. For larger radii, r, the dose is assumed to behave like $1/r^2$. The center radius, R_c; the penumbra radius, R_p; the constant center dose, D_c; and the penumbra dose, D_p, as a function of track radius, r (μm), are given as follows:

$$R_c = 0.01 \quad [\mu\text{m}], \tag{21}$$

$$R_p = 0.05\left(\frac{E}{A}\right)^{1.7} \quad [\mu\text{m}], \tag{22}$$

$$D_C = \frac{1}{\pi R_c^2}\left(\frac{LET_\infty}{\rho[1 + 2\ln(R_p/R_c)]}\right), \tag{23}$$

$$D_p(r) = \frac{1}{\pi r^2}\left(\frac{LET_\infty}{\rho[1 + 2\ln(R_p/R_c)]}\right). \tag{24}$$

Figure 1 shows a comparison of the Kiefer–Chatterjee track structure model and the LEM-oriented track structure model in the case of a carbon-ion beam with an energy of 43 MeV/u and an LET of 50 keV μm^{-1}. In the case of the LEM-oriented track structure model, the local dose in the penumbra region increases, and the dose in the center region is smaller than that of the Kiefer–Chatterjee track structure model.

2.3. Single-event dose mean specific energy

In the MKM, the single-event dose mean specific energy of the domain and the nucleus is necessary for calculating survival curves. The domain and nucleus were assumed to be cylindrical for the sake of simplifying the calculations, and the amorphous track structure model was used. The energy imparted to the cylindrical volume was calculated in accord with the following assumptions:

(a) the paths of incident ions were parallel to the cylindrical axis of the sensitive volume;
(b) changes in the ion trajectory and speed during the passage could be neglected;

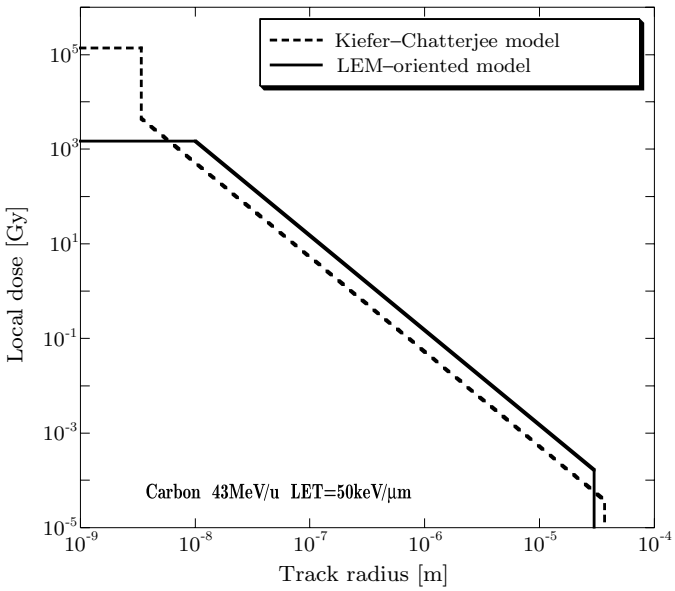

Figure 1. Two track structures for a carbon-ion beam with an energy of 43 MeV/u and a LET of 50 keV μm^{-1}. The solid line was obtained by the LEM-oriented model. The dotted line was calculated by the Kiefer–Chatterjee model.

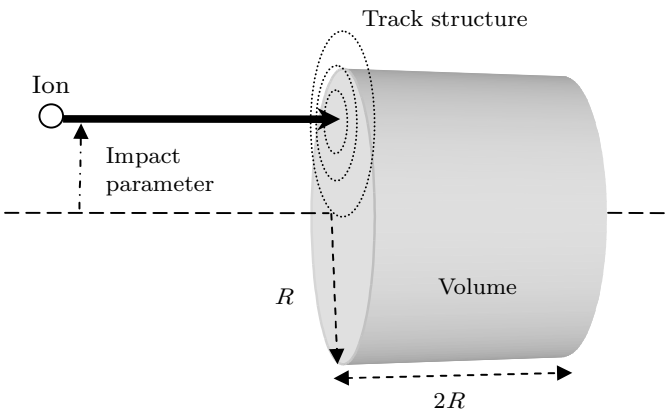

Figure 2. Schematic of an incident ion with respect to a cylindrical sensitive volume.

(c) the ions constantly produced the averaged dose track structure, depending on the particle type and energy; and
(d) the whole target was assumed to be composed of water.

Figure 2 is a schematic diagram of an incident ion with respect to the cylindrical sensitive volume. Figure 3 shows the specific energy in volumes of the cylindrical radius of 0.1, 0.3 and 1.0 μm, respectively, as a function of the impact parameter of the incident ^{12}C ion with an energy of 43 MeV/u, as calculated according to the Kiefer–Chatterjee track structure model. The larger the cylindrical radius of the domain, the smaller the specific energy the domain exhibits around the center region in the track. The domain assumed in the MKM disperses

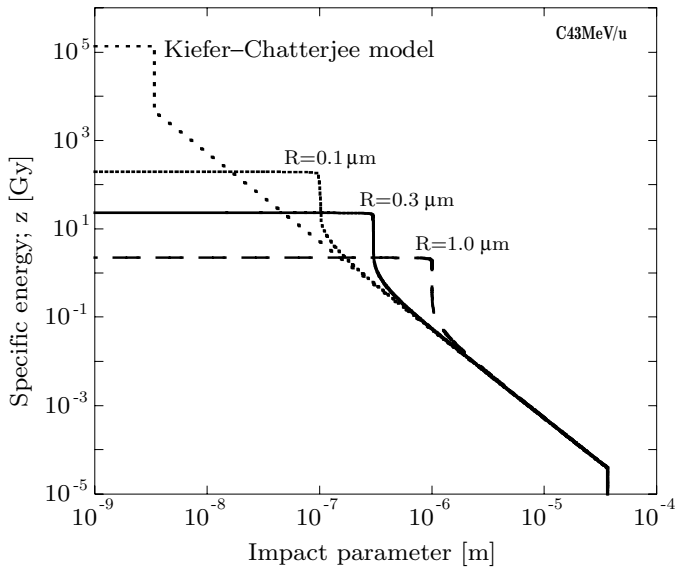

Figure 3. Specific energy in cylindrical radius volumes of 0.1, 0.3 and 1.0 μm, as a function of the impact parameter for a carbon-ion beam with an energy of 43 MeV/u and a LET of 50 keV μm^{-1}, calculated based on the amorphous track structure of the Kiefer–Chatterjee model.

the energy depositions around the track core into the entire domain volume, and thus the domain operates as if it reduces the biological effect at the extremely high local dose in the ion track.

The single-event dose mean specific energy, z_{1D}, was derived from the relationship between the impact parameter, x, and the specific energy, $z(x)$, as follows:

$$z_{1D} = \frac{\int_0^{X_m} z(x)^2 \cdot 2\pi x \, \mathrm{d}x}{\int_0^{X_m} z(x) \cdot 2\pi x \, \mathrm{d}x}, \tag{25}$$

where X_m indicates the maximum impact parameter possible to obtain an energy deposition into the sensitive volume. In this study, the X_m value is the penumbra radius of the track plus the cylindrical radius of the sensitive volume.

2.4. Approximations applied to the LEM

In the implementation of the LEM throughout this study, we use the approximations presented by Scholz *et al* (1997) and Krämer and Scholz (2006), which significantly speed up the calculations although these approximations are not necessary for determining the response to heavy ion irradiation. Namely, the average number of lethal events $\langle L_{\mathrm{nucl}} \rangle$ used in equation (16) is calculated from a central particle traversal. Additionally, a simple relation between α^* and α is exploited to determine an approximation of the quadratic parameter β, which is not constant, in contrast to that of the MKM.

2.5. The modified LEM

Thus far, only the original LEM has been used in treatment planning for carbon-ion therapy. However, a modified version of the LEM was recently introduced (Elsässer and Scholz 2007),

Table 1. Parameters in the MKM calculation using the Kiefer–Chatterjee model.

Cell type	α_0 (Gy^{-1})	β (Gy^{-2})	R_d (μm)	R_n (μm)
HSG	0.313	0.0615	0.34	4.1
V79	0.184	0.02	0.26	4.1
T1	0.0305	0.0585	0.35	3.5

and this modified version takes clustering of single-strand breaks into account. The resulting additional damage leads to greater damage at the track center, and therefore increases the calculated RBE for high-LET particles. Additionally, the radial dose distribution was refined by convolving the dose distribution of equations (22)–(24) with a two-dimensional Gaussian function with a width of 4 nm, thereby representing the radical diffusion length in mammalian cells. The radius of equation (21) was reduced to $R_c = 0.3$ nm, since the radical diffusion is explicitly modeled by the newly implemented Gaussian function. The maximum radius is parameterized by $R_p = 0.062 \cdot E^{1.7}$ [μm].

3. Results

3.1. MKM calculation

We used the survival curves of *in vitro* HSG, V79 and T1 tumor cells irradiated by ^{3}He-, ^{12}C- and ^{20}Ne-ion beams under aerobic conditions (Furusawa *et al* 2000) to examine the MKM calculations. The LET ranges of these beams were 18.6–91 keV μm^{-1} for ^{3}He ions with an initial kinetic energy of 12 MeV/u, 22.5–432 keV μm^{-1} for ^{12}C ions with 12 MeV/u or 135 MeV/u and 62–570 keV μm^{-1} for ^{20}Ne ions with 135 MeV/u. We calculated these survival curves from the MKM with the biological parameters and the track structure to compare the results of the MKM calculation with the biological data. Because the energy straggling in the range shifter and the fragmentation were negligibly small, the distribution of the LET value was ignored in the MKM calculations, such that the dose-averaged LET was equal to the unrestricted LET calculated by the Bethe–Bloch formula. The α_0 and β values were assumed to be the same as the α and β values obtained with 200 kVp x-rays under aerobic conditions, because the z_{1D} value for the x-rays in equation (4) was thought to be negligibly small relative to that for heavy-ion beams.

Ten per cent survival doses were obtained in order to compare the published biological data with the results of the MKM calculations under various conditions. Figure 4 shows the domain radius dependence of D_{10} values as a function of LET for the ^{12}C-ion beams, which was calculated according to the MKM with the α_0 and β values for the aerobic HSG cells and by the Kiefer–Chatterjee track structure model. Figure 5 shows the nuclear radius dependence of the D_{10} values obtained in the same manner as a function of LET for ^{12}C-ion beams. The nuclear radius was set to 3.0, 4.1 and 5.0 μm, respectively. Figure 6 shows the D_{10} values of the HSG, V79 and T1 cells under aerobic conditions as a function of the dose-averaged LET for the ^{3}He-, ^{12}C- and ^{20}Ne-ion beams, where a comparison of the biological results with those obtained by the MKM calculations using the Kiefer–Chatterjee track structure was carried out. Table 1 provides a summary of the biological MKM parameters fitted to calculate the cell survival curves for each cell type. The MKM explained the LET dependence of the biological effects of cell killing and the ion-type dependence of the LET-D_{10} relation. In addition, the MKM calculations based on the Kiefer–Chatterjee track structure model showed good agreement with the biological results for monochromatic ^{3}He-, ^{12}C- and ^{20}Ne-ion beams.

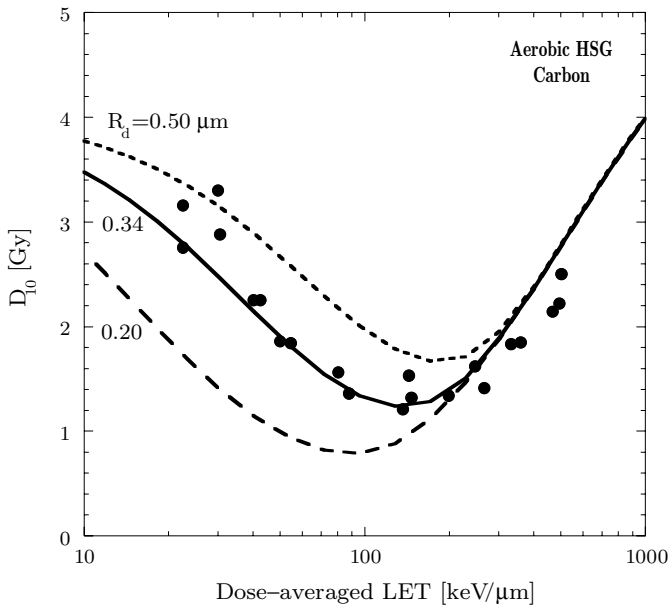

Figure 4. Domain radius dependence of D_{10} values as a function of LET for ^{12}C-ion beams, which was calculated by the MKM with the α_0 and β values for aerobic HSG cells and by the Kiefer–Chatterjee track structure model. In the MKM calculations, the domain radius was set to 0.50, 0.34 or 0.20 μm, with a fixed nuclear radius of 4.1 μm. The closed circles indicate the experimental results of aerobic HSG cells for ^{12}C-ion beams (Furusawa *et al* 2000).

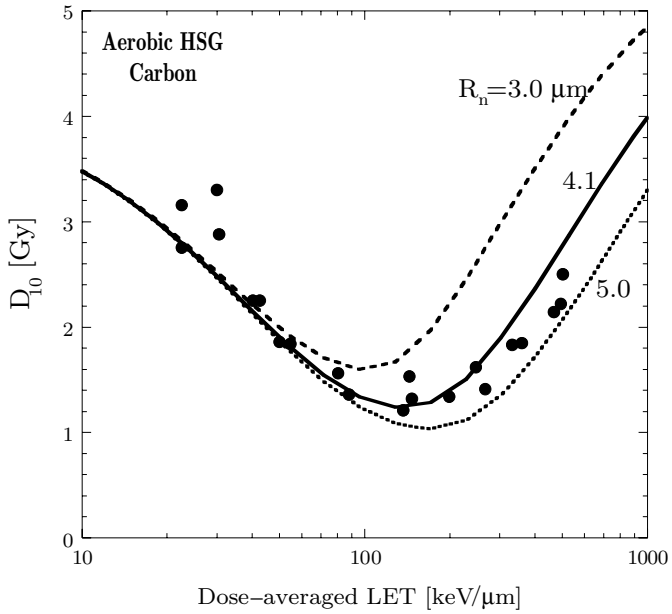

Figure 5. Nuclear radius dependence of D_{10} values as a function of LET for ^{12}C-ion beams, which was calculated by the MKM with the α_0 and β values for aerobic HSG cells and by the Kiefer–Chatterjee track structure model. In the MKM calculations, the nuclear radius was set to 3.0, 4.1 and 5.0 μm, with a fixed domain radius of 0.34 μm. The closed circles indicate the experimental results of aerobic HSG cells for ^{12}C-ion beams (Furusawa *et al* 2000).

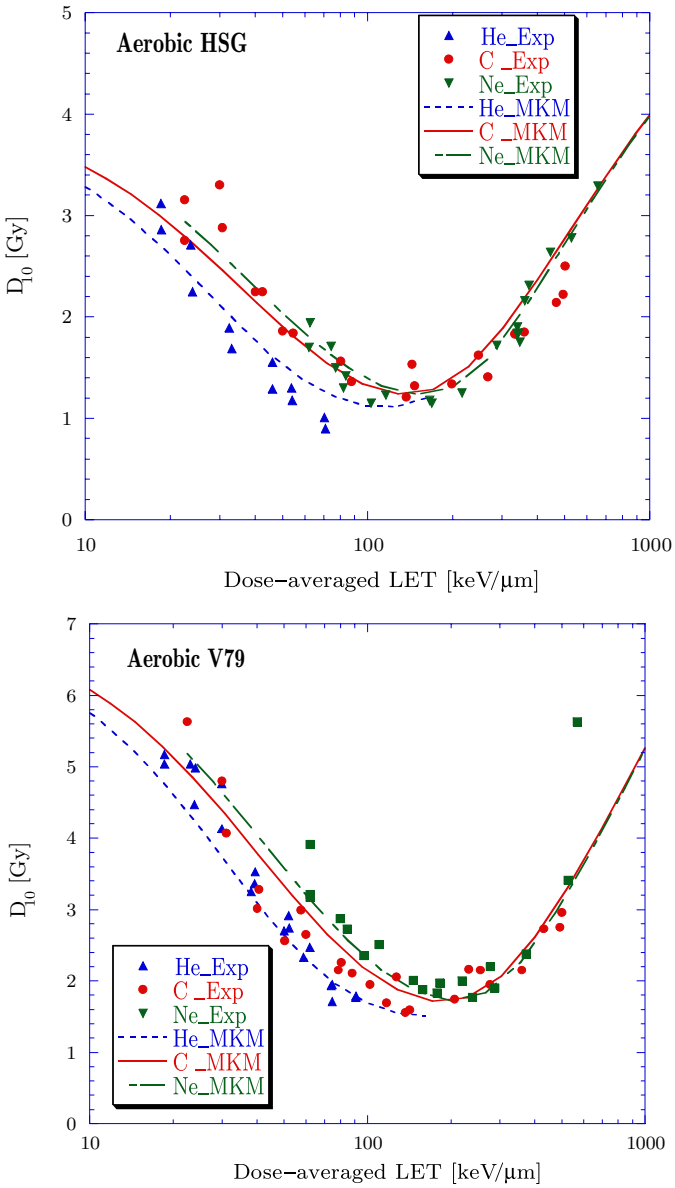

Figure 6. D_{10} values of HSG, V79 and T1 cells under aerobic conditions as a function of dose-averaged LET for ^{3}He-, ^{12}C- and ^{20}Ne-ion beams. The plotted points indicate the experimental results (Furusawa *et al* 2000). The lines represent the MKM calculations carried out with the Kiefer–Chatterjee track structure model.

The LEM-oriented track structure model was also used to compare the MKM calculations with the same experimental data. Figure 7 shows the D_{10} values of the HSG cells under aerobic conditions as a function of the dose-averaged LET for ^{3}He-, ^{12}C- and ^{20}Ne-ion beams; this figure compares the biological results with the results of the MKM calculations using the LEM-oriented track structure. Since track structure affects the MKM calculations, the domain radius of 0.17 μm was used for the aerobic HSG cells in order to fit the data to the biological

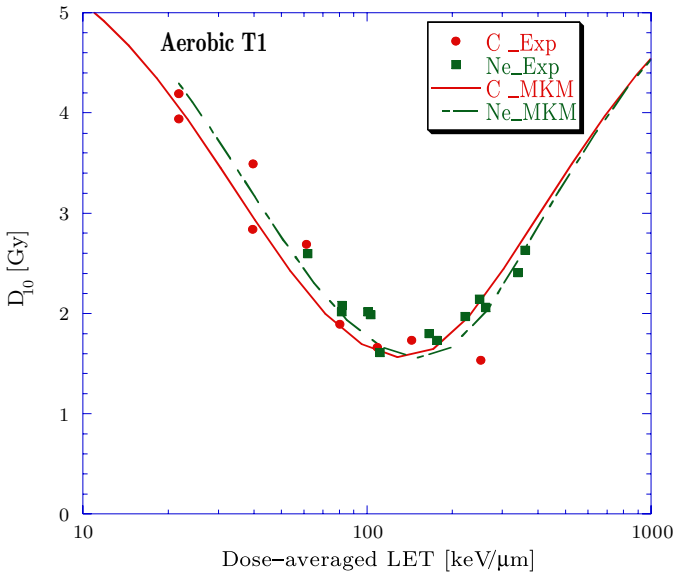

Figure 6. (Continued.)

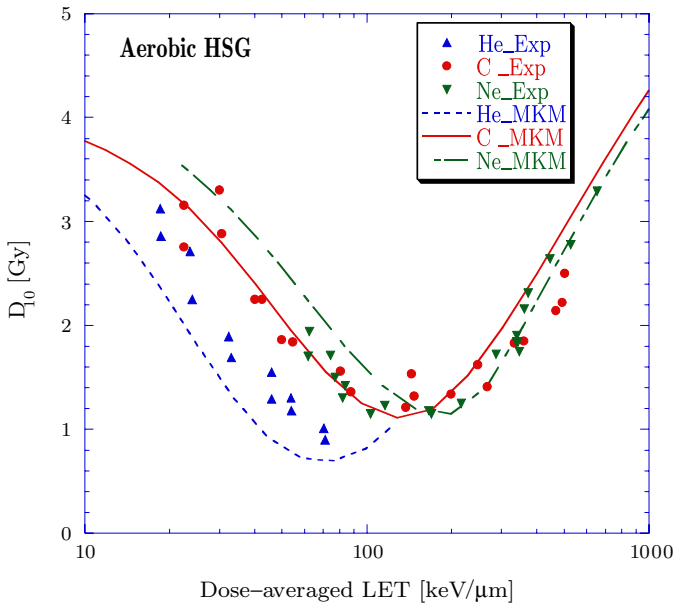

Figure 7. D_{10} values of HSG cells under aerobic conditions as a function of dose-averaged LET for ^{3}He-, ^{12}C- and ^{20}Ne-ion beams. The plotted points indicate the experimental results (Furusawa *et al* 2000). The lines represent the MKM calculations carried out with the LEM-oriented track structure model.

results, although the same three MKM parameters, α_0, β and R_n, were used as given in table 1.

According to the MKM results using the LEM-oriented track structure, the gaps in the LET–D_{10} relationship among the ^{3}He-, ^{12}C- and ^{20}Ne-ion beams were too large compared to

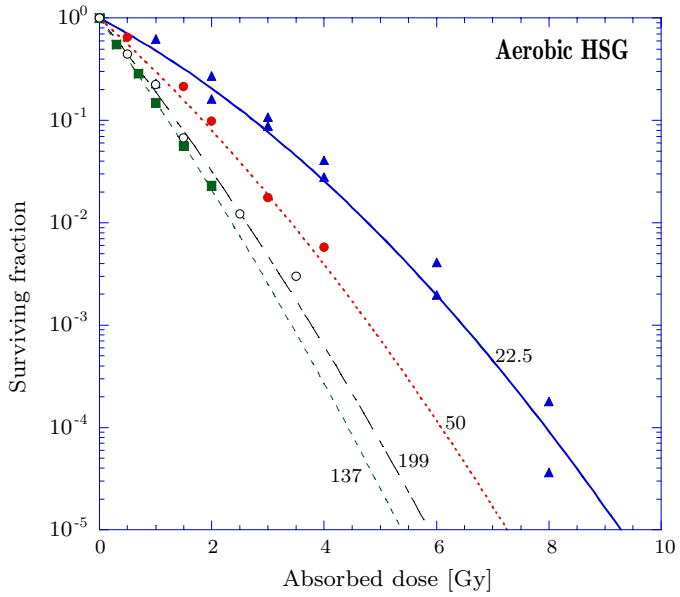

Figure 8. Survival curves of aerobic HSG cells for ^{12}C-ion beams with a dose-averaged LET of 22.5, 50.0, 137 or 199 keV μm^{-1}. The plotted points indicate the experimental results (Furusawa *et al* 2000) and the lines represent the MKM results calculated with the Kiefer–Chatterjee track structure model.

the gaps in the experimental data, although the curve of the LET–D_{10} relation for the ^{12}C-ion beams approximated the biological results. Thus, the difference due to the track structure model exerted a clear influence on the gaps of the LET–D_{10} relation among different ions, and so the ion-type dependence of the LET–RBE relationship is thought to be due to the track structure.

Figure 8 indicates the surviving fraction of aerobic HSG cells as a function of the absorbed dose for ^{12}C-ion beams with a dose-averaged LET of 22.5, 50.0, 137 or 199 keV μm^{-1} and the calculated results by the MKM calculation using the Kiefer–Chatterjee model. The comparison demonstrates that the MKM is capable of predicting cell inactivation over the entire dose range relevant for experimental studies.

3.2. LEM calculation

The survival curves of the aerobic HSG cells were also calculated by the LEM. The LEM parameters, α_x and β_x, are the LQ model parameters for x-rays, and thus these were the same values as the MKM parameters, α_0 and β, indicated in table 1.The nuclear radius of 5.0 μm was used for the LEM calculations (Elsässer and Scholz 2007). We assumed that the threshold dose, D_t, was an adjustable parameter due to the difficulty of obtaining the D_t value from the empirical survival curve for x-rays.

Figure 9 shows the D_{10} values of the aerobic HSG cells as a function of the dose-averaged LET for the ^{12}C-ion beams as compared to the results of calculations carried out with the Kiefer–Chatterjee track structure model, which is not the model actually used in all representations of the LEM. The comparison made here is merely to show the influence of a different radial dose distribution. The D_t values were set to 5, 10, 20, 30 and 50 Gy in the LEM calculations. For all D_t values under investigation, the calculations hardly fit with

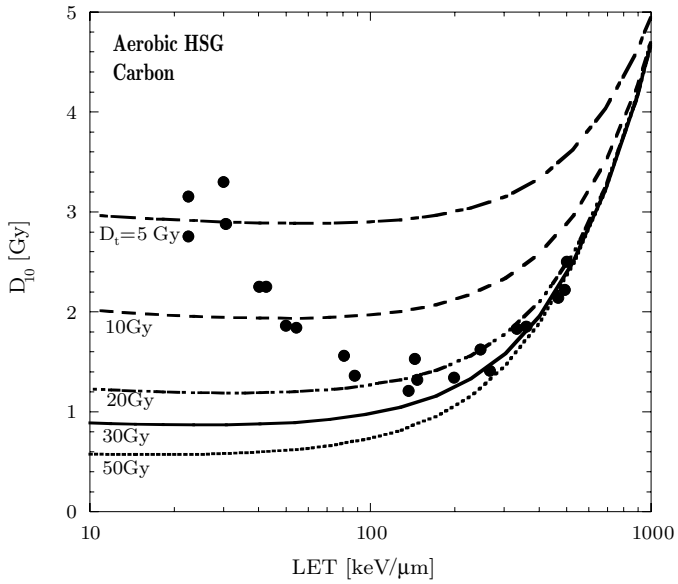

Figure 9. D_{10} values of HSG cells under aerobic conditions as a function of dose-averaged LET for ^{12}C-ion beams. The plotted points indicate the experimental results (Furusawa *et al* 2000). The lines represent calculations based on the LEM principles, but with the Kiefer–Chatterjee track structure model, which is different from the track structure used in the LEM. The threshold dose, D_t, was set to 5, 10, 20, 30 or 50 Gy.

the experimental D_{10} values of aerobic HSG cells. This result is not surprising, since the Kiefer–Chatterjee track structure does not take into account radical diffusion, which reduces the highest and most efficient local doses in the track center.

Figure 10 shows the D_{10} values of aerobic HSG cells as a function of the dose-averaged LET for the ^{12}C-ion beams, as compared to the results of the LEM calculation carried out with the LEM-oriented track structure model. The D_t values were set to 5, 10, 20, 30 and 50 Gy in the LEM calculation.

As expected, the LEM calculation depends largely on the track structure and the LEM-oriented track structure model gave results close to the experimental values. Figure 11 shows the D_{10} values of aerobic HSG cells as a function of the dose-averaged LET for the ^{3}He-, ^{12}C- and ^{20}Ne-ion beams, as compared to the corresponding values obtained by LEM calculations with the LEM-oriented track structure model and 30 Gy for the D_t value. The results of the LEM calculation agreed quite well with the biological results for ^{12}C-ion beams; however, the difference between simulations and experimental results obtained with ^{3}He- and ^{20}Ne-ion beams was larger. In the modified version of the LEM, it was found that the cluster extension and the refined track structure model gave much better agreement of the simulation and the experimental data for He, C and Ne ions (figure 12).

3.3. Direct comparison of the LEM and MKM

Chinese hamster ovary (CHO) cells have frequently been used to test the accuracy of LEM calculations (Scholz *et al* 1997) and predict the biologically effective dose equivalent for carbon therapy at GSI (Krämer and Scholz 2000). Figure 13 shows the 1%, 10% and 50% survival doses of CHO cells using carbon track-segment irradiation (Weyrather *et al* 1999) as a

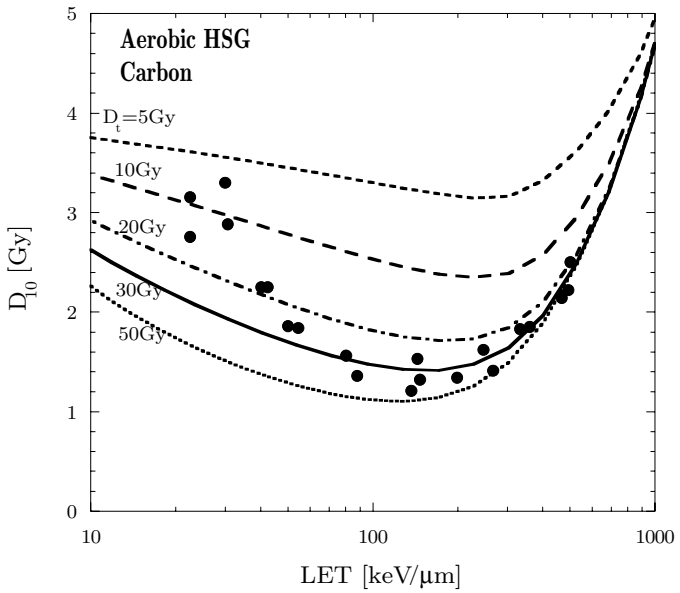

Figure 10. D_{10} values for aerobic HSG cells as a function of dose-averaged LET for ^{12}C-ion beams. The plotted points indicate the experimental results (Furusawa *et al* 2000). The lines represent the LEM calculation. In the LEM calculation, the LEM-oriented track structure model was used, and the threshold dose, D_t, was set to 5, 10, 20, 30 or 50 Gy.

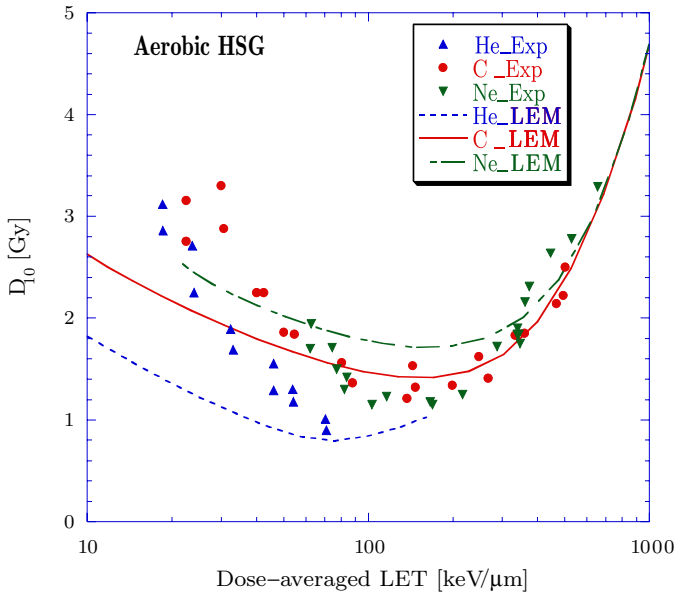

Figure 11. D_{10} values of aerobic HSG cells as a function of dose-averaged LET for ^{3}He-, ^{12}C- and ^{20}Ne-ion beams. The plotted points indicate the experimental results (Furusawa *et al* 2000). The lines represent the LEM calculation carried out with the LEM-oriented track structure model.

function of LET. This series was carried out in order to compare the results obtained by MKM calculations using the Kiefer–Chatterjee track structure model with results obtained with the

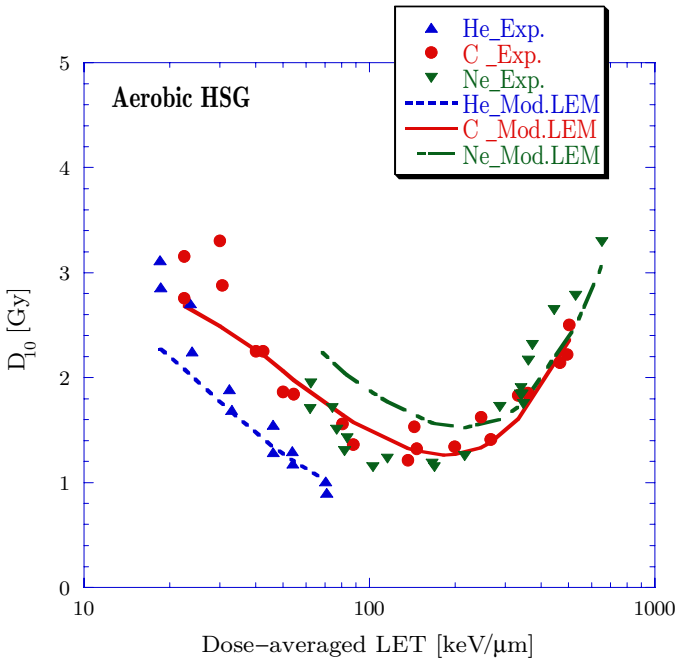

Figure 12. D_{10} values of aerobic HSG cells as a function of dose-averaged LET for ^{3}He-, ^{12}C- and ^{20}Ne-ion beams. The plotted points indicate the experimental results (Furusawa *et al* 2000). The lines represent the modified LEM calculation.

original and modified LEM calculations using the LEM-oriented track structure model. MKM parameters for CHO cells ($\alpha_0 = 0.228$ Gy^{-1}, $\beta = 0.02$ Gy^{-2}, $R_{dl} = 0.2$ μm, $R_n = 4.1$ μm) and LEM parameters for CHO cells ($\alpha_x = 0.228$ Gy^{-1}, $\beta_x = 0.02$ Gy^{-2}, $D_t = 40$ Gy (original), $D_t = 9.5$ Gy (modified), $R_n = 4.7$ μm) (Elsässer and Scholz 2007) were used for these calculations. MKM calculations were found to reflect the 1%, 10% and 50% survival doses of CHO cells using carbon track-segment irradiation, and reasonably good agreement between the results of the LEM calculations and the biological results for all LETs other than 100 and 150 keV μm^{-1} was observed for all survival levels. A relatively large mismatch between experimental and simulation results was observed for 100 and 150 keV μm^{-1} at survival levels of 10% and 1%, respectively. The modified LEM partly compensates for this deficiency, although the biological effectiveness for low-LET particles was underestimated in this particular series. For other cell lines such as HSG cells (depicted in figure 12), and according to the findings of other cellular experiments more closely related to therapy (Krämer *et al* 2003), the agreement of high-LET particles representative for the spread-out Bragg peak with experimental data was much better, whereas the effectiveness of low-LET radiation has been overestimated to some extent.

3.4. Application of MKM and LEM for proton and deuteron beams

The RBE value for the 10% survival level of V79 cells for H- and He-ion beams was also calculated by both models. The MKM uses the parameters summarized in table 1. The LEM uses the same photon LQ parameters: $D_t = 5.5$ Gy and $R_n = 4$ μm. The D_t parameter is different from that used in Elsässer and Scholz (2006), where 15 Gy was found to give the best

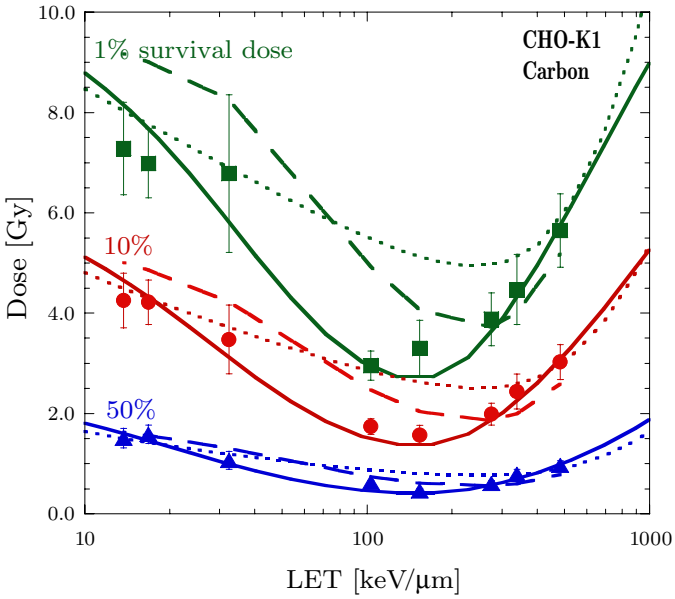

Figure 13. 1%, 10% and 50% survival doses of CHO cells as a function of LET for ^{12}C-ion beams. The closed square, circle and triangle symbols respectively show the 1%, 10% and 50% survival doses of the experimental results, for which the survival doses and error bars were calculated based on the LQ model parameter: α and β values with these uncertainty values (Weyrather *et al* 1999). The solid lines indicate the 1%, 10% and 50% survival doses calculated by the MKM using the Kiefer–Chatterjee track structure model. The dotted lines show the LEM calculation with the LEM-oriented track structure model. The dashed lines represent the modified LEM calculation.

agreement for the carbon data of Furusawa *et al* (2000). In order to facilitate a meaningful comparison, we decided to take the same input parameters for the x-ray survival curves for all experimental data although the authors report different values. Figure 14 shows the results of the MKM and the LEM in its modified version and a comparison to experimental data (Folkard *et al* 1996, Belli *et al* 1998, Furusawa *et al* 2000). The LET–RBE curve for deuterons was almost the same as for protons in the MKM calculation; for the LEM the differences are slightly larger. The experimentally determined RBE for protons (Belli *et al* 1998) decreases for LET values above 30 keV μm^{-1}. It is probably because the assumption of constant ion energy is incorrect for such slow projectiles. Therefore, it was found that both models agree well also for protons and deuterons.

4. Discussion

4.1. Conceptual comparison of LEM and MKM

4.1.1. General aspects. The concept of both models follows the main constituents presented previously in a similar manner by Katz *et al* (1971), and later in the first representation of the LEM (Scholz and Kraft 1996), namely, the survival curve after photon irradiation, the amorphous track structure and the cell nucleus as sensitive target. In the case of the MKM, this cell nucleus is partitioned into cylindrical domains, each with a diameter of a fraction of a micrometer. The differences between the MKM and LEM can be primarily attributed to differences in the respective descriptions of the track structure and the survival curve.

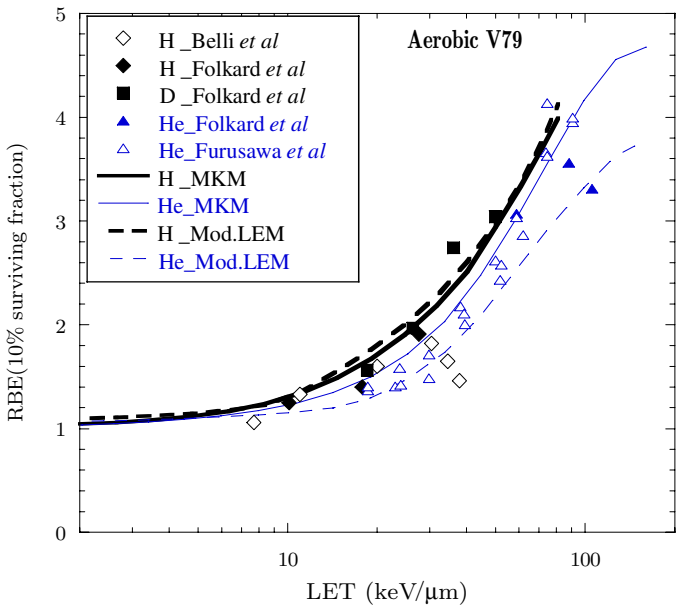

Figure 14. 10% survival RBE of V79 cells as a function of LET for H- and He-ion beams. The plots show the experimental data of V79 cells (Folkard *et al* 1996, Belli *et al* 1998, Furusawa *et al* 2000). The solid lines indicate the MKM calculation with the MKM parameter of V79 cells ($\alpha_0 = 0.184$ Gy^{-1}, $\beta = 0.02$ Gy^{-2}, $R_{dl} = 0.26$ μm, $R_n = 4.1$ μm) and by the Kiefer–Chatterjee track structure model. The dashed lines represent the modified LEM calculation.

4.1.2. Track structure. In the present study, two different representations of the amorphous track structure have been utilized. Here, a formulation according to a mixture of the Kiefer approximation of the penumbra region and the Chatterjee assumptions for the core region was introduced, and this formulation appears to be the most appropriate option for application with the MKM. The high local dose in the track core as given by the Kiefer–Chatterjee model is dispersed due to the concept of the microdosimetric domain yielding to reasonable average numbers of lethal events. In contrast, in the LEM, the Kiefer–Chatterjee model is not applicable due to the lack of radical diffusion and the correspondingly much higher doses in the track center. Neglect of diffusion of radicals is not important in the case of the MKM, since the domain size is much larger than the radical diffusion length. Moreover, the LEM track structure follows the description of the Kiefer model for the outer region of the track, but assumes a constant dose level at the track center, which is dispersed due to radical diffusion.

4.1.3. Photon dose response curve. Additionally, in the LEM and the MKM, the models for cell survival differ. In the MKM, a pure linear-quadratic form is assumed for the entire range of doses, whereas for large doses, the LEM uses a threshold dose to account for the linear behavior of survival curves. In the case of the LEM, the choice is justified by the experimental evidence that inactivation curves gradually tend to become linear (Fertil *et al* 1994, Alpen 1990). However, survival curves have been reported that showed a good fit using the pure LQ model for high doses (Ando *et al* 1992, Fukutsu *et al* 1997). It therefore remains difficult to unequivocally determine which model is correct.

Formally, at doses larger than the threshold dose D_t, either approach can be transformed into the other by conversion of the local dose, d (relevant for the LQ + threshold model), into

a local dose, d' (relevant for the pure LQ model). By assuming that both descriptions will ultimately give the same biological effect, this requires that

$$\alpha_X d' + \beta_X d'^2 = (\alpha_X + 2\beta_X D_t)d - \beta_X D_t^2 \qquad (d > D_t), \tag{26}$$

and thus,

$$d' = \frac{1}{2\beta}\left(\sqrt{\alpha^2 + 4\beta\left(\beta D_t^2 - \{\alpha + 2\beta D_t\}d\right)} - \alpha\right) \qquad (d > D_t). \tag{27}$$

4.1.4. Relation of different photon dose response representations and track structure. Directly calculating the biological effect from the local dose in the track based on the pure linear-quadratic model would result in inactivation probabilities that would be too high, compared to the experimental values, for both the MKM as well as for the LEM approach. Therefore, the MKM determines the biological effect based on the *average dose* in a micrometer-sized domain, thereby reducing the biological effect. However, due to the averaging procedure, the MKM is less sensitive to the details of the track structure on the order of nanometers, i.e., at the center of the track. In the LEM, the local dose is directly converted to a local biological effect without averaging of the dose over an extended target volume; the assumption of a straight exponential shape of the photon dose response curve for high doses thus gives consistent results.

Therefore, the assumptions regarding the shape of the photon dose response curve and the target volume for the determination of the biological effect are strongly coupled in both models. Neither the MKM with a LQ + threshold representation, nor the LEM with a pure LQ representation is able to correctly predict the survival probabilities by using the radial dose profiles shown in figure 2. In that case, agreement between the model predictions and the experimental results would be possible only if modifications of the radial dose profile were used, and these modifications are inconsistent with experimental/modeling data on the track structure. For example, in the case of the LEM, the local dose at the track center must be significantly reduced, as demonstrated in figure 15, with the consequence that the integral of the dose distribution differs significantly from the LET, in contrast to the principle of energy conservation. Figure 15 illustrates an example of the converted d' distribution according to equation (27) using the LEM parameters for aerobic HSG cells, i.e., $\alpha_x = 0.313$ Gy^{-1}, $\beta_x = 0.0615$ Gy^{-2} and the D_t values of 1, 30 or 100 Gy corresponding to the LEM-oriented track structure in a 43 MeV/u ^{12}C-ion track with 50 keV μm^{-1} in LET. The conversion from d to d' in the region of d values higher than D_t formally corresponds to the reduction of the local dose, if we assume that the linear-quadratic model for inactivation holds for all doses. In the case of $D_t = 30$ Gy, for example, the modified value of $d' = 300$ Gy leads to the same average number of lethal events, as in the case when D_t is applied in the survival curve according to equation (8), without correction for a local dose of 1500 Gy. In contrast, assuming that the LQ + threshold model is the valid representation of the photon dose response curve, in the case of the MKM, the values of the local dose would have to be considerably increased in order to achieve a reasonable representation of the experimental survival data. This would lead to domain radii smaller than the values depicted in figure 3.

According to the considerations above, we find that a conversion of the input photon survival curves into each other is mathematically possible, but such conversion results either in incorrect predictions with respect to the experimental data or in illegitimate assumptions for the track structure.

4.1.5. Target definition. Both models use the same approximation of the correction for high-LET particles due to the non-Poisson distribution of lethal events. This correction requires

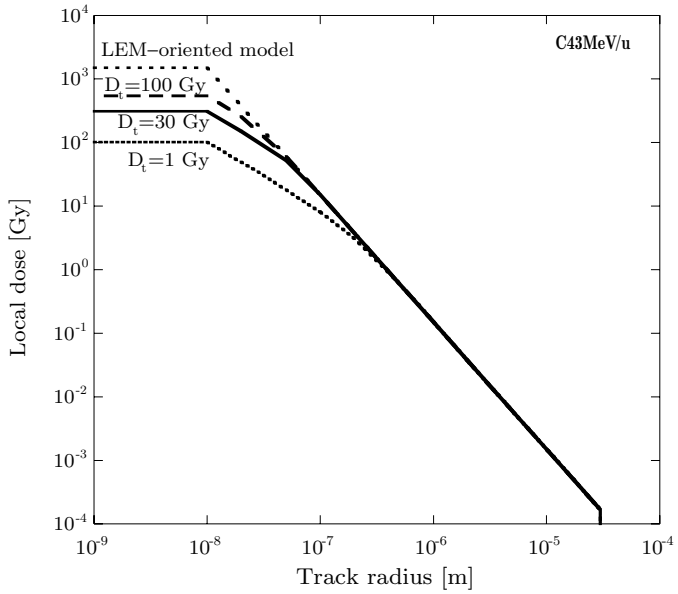

Figure 15. Converted d' distribution assuming a pure linear-quadratic photon response curve corresponding to the LEM-oriented track structure and using the LEM parameters for aerobic HSG cells; $\alpha_x = 0.313$ Gy^{-1}, $\beta_x = 0.0615$ Gy^{-2} with a D_t value of 1, 30 or 100 Gy in a 43 MeV/u ^{12}C-ion track with an LET of 50 keV μm^{-1}.

that the nuclear dimension be the target size in order to determine the hit statistics. However, the method used to determine the nuclear radius differs between models. In the case of the LEM, the effective nuclear radius is calculated based on measurements of the distribution of the nuclear area (Scholz and Kraft 1996), taking into account the finite distribution of nuclear sizes. In the MKM, the radius is assumed to fit the experimental results regardless of the size distribution.

4.1.6. Definition of input parameters. The most significant difference between the MKM and the LEM is related to the definition of the input parameters. In the LEM, all parameters are, at least in principle, defined by measurable quantities. The most critical parameter here is the threshold dose D_t, since it is practically difficult to precisely determine the photon dose response curve at very high doses. Thus, D_t is usually kept as an adjustable parameter in order to allow the best representation of the experimental data. However, from a conceptual point of view, D_t represents a measurable quantity. In contrast, in the MKM, the domain size, a critical parameter, does not currently represent a measurable quantity, since it cannot be uniquely identified with any known structure in the cell or cell nucleus. The domain size is a means of adjusting the number of lethal events in combination with the photon survival curve. The dependence of the results on the adjustable parameters of the models (figures 4 and 10) reveals that the MKM predictions are slightly more sensitive to relative variations of the domain size than are the LEM results with respect to the choice of D_t.

4.2. Application of models in treatment planning

As shown in the section 3, both models provide a good description for different sets of experimental data. For some LET–energy combinations, the agreement with the experimental

results is better with the MKM. There is a tendency for overestimation of RBE by the LEM model for high energetic ions at comparably low LET. Consequently, when applied in treatment planning, the effective dose in the normal tissue surrounding the tumor can be expected to be lower than predicted by the LEM. With regard to normal tissue tolerance, this is a safe situation, since the complication probability is lower than predicted by the model. However, this systematic has to be kept in mind when, e.g. comparing effective dose distributions for carbon ions versus protons or when prescribing the absolute treatment dose.

The implementation of the amorphous track structure in the MKM as presented in this paper is a big step in terms of application for treatment planning with a wide range of ions and energies and represents an important extension of the original MKM approach.

Their simplicity and the computational speed render both of these models important tools for planning heavy-ion tumor therapy. As regards the LEM, it has been demonstrated to be capable of predicting the *in vivo* response as well as that of complex tissues based on the finding that the α/β ratio of the photon dose response curve is the major determinant of the RBE; thus, for tissues with a given α/β ratio, RBE values similar to those of a photon cell survival curve with the same α/β ratio can be expected (Scholz 1996). For example, the RBE for the skin reaction in minipigs has been prospectively calculated using the LEM and could be shown to represent the experimental data with sufficient accuracy (Zacharias *et al* 1997). Similarly, the general systematic of RBE for the tolerance of the rat spinal cord can be described with the LEM, although an underestimation of the RBE for Bragg peak irradiation has been found (Karger *et al* 2006). However, this underestimation is not seen in the TCP data for skull-base chordomas (Schulz-Ertner *et al* 2007). Here the clinical TCP values very well coincide with the extrapolation from photon and proton data when plotted as a function of the isoeffective dose, which was calculated using the LEM. Similarly, the LEM has been shown to correctly represent the TCP curve for non-small cell lung cancer (Scholz *et al* 2006). Further systematic investigation of the MKM model will be required in order to demonstrate that it is applicable for predicting tissue responses as well.

5. Conclusions

The cell survival curves of *in vitro* cells irradiated by ^{3}He-, ^{12}C- and ^{20}Ne-ion beams were calculated using the MKM and LEM. It was found that the MKM calculation using the Kiefer–Chatterjee track structure model was closest to the experimental results. Similarly, the LEM gave also good results for a wide range of parameters, especially in its modified version. In our consideration of the amorphous track structure model, we demonstrated that the differences between the results obtained with MKM and LEM are primarily due to different means of calculating the biological effect of an extremely high local dose at the center of the ion track. These different approaches reflect the different biological, physical and chemical justifications of the respective models, as expressed in terms of (experimental) parameters such as the central track region, threshold parameter and radical diffusion length on the one hand, and the domain size and core radius on the other hand.

A strength of both models is that due to the simplicity and the computational speed of the calculations, they are both applicable for treatment planning. If the photon dose response for the corresponding tissue is known, the ion response for all parameters is calculated immediately. In either case, additional information about the biological response to ion irradiation is necessary to determine the domain size or the threshold dose. In the case of the LEM, two selected RBE values for low and high LET particles, respectively, are sufficient for this purpose. Additionally, similar photon survival curves with the same or a similar α/β ratio yield similar results with respect to the ion response.

In summary, the MKM and the LEM rely on the same three basic constituents of target geometry, photon survival curve and track structure; however, their implementation of these constituents is significantly different.

References

Alpen E L 1990 Radiation biophysics *Prentice Hall Advanced Reference Series* (Englewood Cliffs, NJ: Prentice-Hall)

Ando K, Koike S and Sato S 1992 Nonlinear survival curves for cells of solid tumors after large doses of fast neutron and γ rays *Radiat. Res.* **131** 157–61

Belli M *et al* 1998 RBE-LET relationship for cell inactivation and mutation induced by low energy protons in V79 cells: further results at the LNL facility *Int. J. Radiat. Biol.* **74** 501–9

Chatterjee A and Schaefer H J 1976 Microdosimetric structure of heavy ion tracks in tissue *Radiat. Environm. Biophys.* **13** 215–27

Elsässer T and Scholz M 2006 Improvement of the Local Effect Model (LEM)—implications of clustered DNA damage *Radiat. Prot. Dosim.* **122** 475–7

Elsässer T and Scholz M 2007 Cluster effects within the local effect model *Radiat. Res.* **167** 319–29

Fertil B, Reydellet I and Deschavanne P J 1994 A benchmark of cell survival models using survival curves for human cells after completion of repair of potentially lethal damage *Radiat. Res.* **138** 61–9

Folkard M, Prise K M, Vojnovic B, Newman H C, Roper M J and Michael B D 1996 Inactivation of V79 cells by low-energy protons, deuterons and helium-3 ions *Int. J. Radiat. Biol.* **69** 729–38

Fukutsu K, Kanai T, Furusawa Y and Ando K 1997 Response of mouse intestine after single and fractionated irradiation with accelerated carbon ions with a spread-out Bragg peak *Radiat. Res.* **148** 168–74

Furusawa Y, Fukutsu K, Aoki M, Itsukaichi H, Eguchi-Kasai K, Ohara H, Yatagai F, Kanai T and Ando K 2000 Inactivation of aerobic and hypoxic cells from three different cell lines by accelerated ^{3}He-, ^{12}C- and ^{20}Ne-ion beams *Radiat. Res.* **154** 485–96

Hawkins R B 1994 A statistical theory of cell killing by radiation of varying linear energy transfer *Radiat. Res.* **140** 366–47

Hawkins R B 2003 A microdosimetric-kinetic model for the effect of non-Poisson distribution of lethal lesions on the variation of RBE with LET *Radiat. Res.* **160** 61–9

Hirao Y, Ogawa H, Yamada S, Sato Y, Yamada T, Sato K, Itano A, Kanazawa M, Noda K and Matsumoto S 1992 Heavy ion synchrotron for medical use -HIMAC project at NIRS-JAPAN *Nucl. Phys.* A **538** 541c–50c

Itano A 1995 Heavy ion medical accelerator project by Hyogo Prefectural Government *Proc. 10th Symp. on Accel. Sci. and Tech. et al* pp 398–400

Kagawa K, Mayahara H, Oda Y, Kawaguchi A, Murakami M, Hishikawa Y and Abe M 2005 Carbon ion radiotherapy for mucosal malignant melanoma of the head and neck *Int. J. Radiat. Oncol. Biol. Phys.* **63** S356

Kanai T, Furusawa Y, Fukutsu K, Itsukaichi H, Eguchi-Kasai K and Ohara H 1997 Irradiation of mixed beam and design of spread-out Bragg peak for heavy-ion radiotherapy *Radiat. Res.* **147** 78–85

Kanai T *et al* 1999 Biophysical characteristics of HIMAC clinical irradiation system for heavy-ion radiation therapy *Int. J. Radiat. Oncol. Biol. Phys.* **44** 201–10

Kanai T, Matsufuji N, Miyamoto T, Mizoe J, Kamada T, Tsuji H, Kato H, Baba M and Tsujii H 2006 Examination of GyE system for HIMAC carbon therapy *Int. J. Radiat. Oncol. Biol. Phys.* **64** 650–6

Karger C P, Peschke P, Sanchez-Brandelik R, Scholz M and Debus J 2006 Radiation tolerance of the rat spinal cord after 6 and 18 fractions of photons and carbon ions: experimental results and clinical implications *Int. J. Radiat. Oncol. Biol. Phys.* **66** 1488–97

Kase Y, Kanai T, Matsumoto Y, Furusawa Y, Okamoto H, Asaba T, Sakama M and Shinoda H 2006 Microdosimetric measurements and estimation of human cell survival for heavy-ion beams *Radiat. Res.* **166** 629–38

Katz R, Ackerson B, Homayoonfar M and Sharma S C 1971 Inactivation of cells by heavy ion bombardment *Radiat. Res.* **47** 402–25

Kellerer M and Rossi H H 1978 A generalized formation of dual radiation action *Radiat. Res.* **75** 471–88

Kiefer J and Straaten H 1986 A model of ion track structure based on classical collision dynamics *Phys. Med. Biol.* **31** 1201–9

Kraft G 2000 Tumor therapy with ion beams *Nucl. Instrum. Methods* A **454** 1–10

Kraft G, Scholz M and Bechthold U 1999 Tumor therapy and track structure *Radiat. Environ. Biophys.* **38** 229–37

Krämer M and Scholz M 2000 Treatment planning for heavy-ion radiotherapy: calculation and optimization of biologically effective dose *Phys. Med. Biol.* **45** 3319–30

Krämer M, Wang J F and Weyrather W 2003 Biological dosimetry of complex ion radiation fields *Phys. Med. Biol.* **48** 2063–70

Krämer M and Scholz M 2006 Rapid calculation of biological effects in ion radiotherapy *Phys. Med. Biol.* **51** 1959–70

Pirruccello M C and Tobias C A 1980 Biological and medical research with accelerated heavy ions at the BEVALAC, 1977–1980 *LBL report 11220* (CA: Lawrence Berkley Laboratory)

Sakama M, Kanai T, Kase Y, Komori M, Fukumura A and Kohno T 2005 Responses of a diamond detector to high-LET charged particles *Phys. Med. Biol.* **50** 2275–89

Scholz M, Kellerer A M, Kraft-Weyrather W and Kraft G 1997 Computation of cell survival in heavy ion beams for therapy *Radiat. Environ. Biophys.* **36** 59–66

Scholz M and Kraft G 1996 Track structure and the calculation of biological effects of heavy charged particles *Adv. Space Res.* **18** 5–14

Scholz M 1996 Calculation of RBE for normal tissue complications based on charged particle tracks *Bull. Cancer Radiother.* **83** 50s–54s

Scholz M, Matsufuji N and Kanai T 2006 Test of the local effect model using clinical data: tumour control probability for lung tumours after treatment with carbon ion beams *Radiat. Prot. Dosim.* **122** 478–9

Schulz-Ertner D, Karger C P, Feuerhake A, Nikoghosyan A, Combs S E, Jäkel O, Edler L, Scholz M and Debus J 2007 Effectiveness of carbon ion radiotherapy in the treatment of skull-base chordomas *Int. J. Radiat. Oncol. Biol. Phys.* **68** 449–57

Tobias C A, Wenke R P and Benton E V 1973 Heavy-particle radiotherapy *Science* **182** 474–6

Weyrather W K, Ritter S, Scholz M and Kraft G 1999 RBE for carbon track-segment irradiation in cell lines of differing repair capacity *Int. J. Radiat. Biol.* **75** 1357–64

Zacharias T *et al* 1997 Acute response of pig skin to irradiation with ^{12}C-ions or 200 kV x-rays *Acta Oncol.* **36** 637–42

Zaider M and Rossi H H 1980 The synergistic effects of different radiations *Radiat. Res.* **83** 732–9